INTERNATIONAL JOURNAL FOR NUMERICAL METHODS IN FLUIDS
Int. J. Numer. Meth. Fluids 2007; **54**:237–268
Published online 30 November 2006 in Wiley InterScience (www.interscience.wiley.com). DOI: 10.1002/fld.1391

Baroclinic stability for a family of two-level, semi-implicit numerical methods for the 3D shallow water equations

Francisco J. Rueda[1,*,†], Enrique Sanmiguel-Rojas[2] and Ben R. Hodges[3]

[1]*Dpto. Ingeniería Civil & Instituto del Agua, Universidad de Granada, C/Ramón y Cajal, 4, Granada 18071, Spain*
[2]*Dpto. Ingeniería Térmica y de Fluidos, Universidad Politécnica de Cartagena, C/Dr. Fleming, s/n, Cartagena 30202, Murcia, Spain*
[3]*Department of Civil, Architectural and Environmental Engineering, University of Texas at Austin, Austin TX 78712-1076, U.S.A.*

SUMMARY

The baroclinic stability of a family of two time-level, semi-implicit schemes for the 3D hydrostatic, Boussinesq Navier–Stokes equations (i.e. the shallow water equations), which originate from the TRIM model of Casulli and Cheng (*Int. J. Numer. Methods Fluids* 1992; **15**:629–648), is examined in a simple 2D horizontal–vertical domain. It is demonstrated that existing mass-conservative low-dissipation semi-implicit methods, which are unconditionally stable in the inviscid limit for barotropic flows, are unstable in the same limit for baroclinic flows. Such methods can be made baroclinically stable when the integrated continuity equation is discretized with a barotropically dissipative backwards Euler scheme. A general family of two-step predictor-corrector schemes is proposed that have better theoretical characteristics than existing single-step schemes. Copyright © 2006 John Wiley & Sons, Ltd.

Received 5 May 2006; Revised 15 September 2006; Accepted 19 September 2006

KEY WORDS: stability analysis; baroclinic terms; two-level semi-implicit methods; 3D shallow water

1. INTRODUCTION

The 3D shallow water equations (SWE herein), also known as the hydrostatic primitive equations, are frequently used to simulate flows in lakes, estuaries and coastal oceans (e.g. [1–3]). Such models

*Correspondence to: Francisco J. Rueda, Dpto. Ingeniería Civil & Instituto del Agua, Universidad de Granada, C/Ramón y Cajal, 4, Granada 18071, Spain.
†E-mail: fjrueda@ugr.es

Contract/grant sponsor: University of Granada

are robust when advection, diffusion, baroclinic, and barotropic components are discretized with numerical methods that are stable in the inviscid limit. An absolutely stable method may be obtained if all terms are discretized implicitly in time; however, such fully coupled implicit solutions of momentum, continuity and density transport have not been proven effective for large-scale natural systems. Some recent progress in fully implicit barotropic solutions indicates future potential [4], but extension to baroclinic flows with implicit coupling of density transport remains an open question. Thus, numerical decoupling of the momentum solution and density transport is used in most models of combined barotropic/baroclinic flows. This decoupling has been generally accomplished in single-step non-iterative methods either by: (1) discretizing explicitly the baroclinic contribution to momentum so that the time '$n+1$' velocity depends only on the density field at time 'n' and earlier (e.g. [1, 5]), or (2) by solving the density transport equations based on time 'n' velocity information, and using the resulting time '$n+1$' density field in the estimates of the baroclinic terms in the momentum equations (e.g. [6, 7]).

Beyond decoupling of density transport and momentum, practical models require some means of addressing the disparity in time scales between the fast barotropic (free surface) waves and the slower baroclinic/advective motions. If the barotropic mode is discretized explicitly, then the time step required for stability is typically so small that the resulting model cannot be practically used for large-scale systems. Common approaches to addressing the time-scale disparity are to use either: (1) a mode-splitting approach (e.g. [5]), with a small time step for explicit time-advance of the barotropic mode and a separate large time step for baroclinic and advective terms or (2) a semi-implicit approach (e.g. [1]), wherein the free surface motion is discretized implicitly while advection and baroclinic solutions are explicit. With the semi-implicit approach, the barotropic Courant number may exceed unity and the solution uses a single time step, whose size is governed by advective and baroclinic Courant–Friedrichs–Lewy (CFL) conditions. Both methods are often combined with an implicit solution for vertical diffusion terms to prevent a diffusive vertical stability limitation.

In the present work, we focus on the semi-implicit method, which has been used a number of recent baroclinic/barotropic flow models (e.g. [2, 8, 9]). It is well-known that formally unstable numerical discretization methods can be used if sufficient viscosity (or diffusion) is added, either directly *via* the viscous (diffusive) terms or indirectly through truncation error in discretizations. It is generally hoped, although not always demonstrated, that such added viscosity/diffusivity causes only minor additions to the physical dissipation/diffusion. However, in flows with strong stratification, reliance on significant added dissipation/diffusion for stabilization can cause problems: stratification may suppress vertical mixing and turbulence, so that the effective turbulent viscosity and diffusivity may be reduced to near-molecular values. In such circumstances, any numerical viscosity/diffusivity required for model stabilization is undesirable. It follows that an ideal numerical discretization of the SWE should be stable in the inviscid limit without artificial viscosity/diffusivity.

We are interested, in particular, in the simplest semi-implicit schemes that have proved both popular and effective: the method of Casulli and Cheng [1], also known in the water resources simulation literature as TRIM (tidal, residual, inter-tidal mudflat). The underlying semi-implicit scheme has been developed extensively by the original author (e.g. [10–13]), has been adapted to POM [5] as the ECOM-siz model [14] and is the basis for the ELCOM model [15]. These models are in wide use throughout the coastal and inland water modelling communities, so their stability characteristics are of wide interest. As originally proposed, the TRIM method can be classified as a 2-level, single-step semi-implicit method. That is, it uses two time-levels of information (n and

DOI: 10.1002/fld

$n+1$) and takes a single model step (from n to $n+1$) to integrate forward in time. This can be contrasted to more complicated semi-implicit 3-level schemes (e.g. [16]) that include time '$n-1$' data; 2-step barotropic predictor-corrector schemes [17] that perform an intermediate estimation step; or the nonlinear-free surface method recently proposed in [7], based on previous work of [6], in which two discrete versions of the continuity equation are solved in the same time step to provide independent estimates of the cell thickness and the dynamic-free surface elevation. The basic TRIM approach solves an integrated implicit solution of the free surface evolution equation (which is formed by integrating continuity and applying the kinematic boundary condition). The resulting free surface is used for the barotropic term in updating the time '$n+1$' velocities. A combination of the computed time '$n+1$' and 'n' velocities and water column elevations are typically used for scalar transport. Casulli and Cattani [10] demonstrated that the TRIM method is unconditionally stable and has minimum dissipation for barotropic flows when the free surface terms are discretized in a centred-time (i.e. Crank–Nicolson) scheme. They further showed that the original backward-time (i.e. backward-Euler) scheme in [1] was extremely dissipative of barotropic motions.

The TRIM model and other models based on the published method have been extensively used in both model development (e.g. [11, 18, 19]) and site-specific studies (e.g. [9, 20–22]) for both barotropic and baroclinic flows. Surprisingly enough, other than a simple baroclinic wave speed CFL limitation noted in [19], the approach has never been analysed to determine the stability, dissipation and phase propagation errors in representation of baroclinic processes. In this paper, we demonstrate that the previously recommended centred-time approach for barotropic discretization in the TRIM family of methods [10] is both theoretically and practically unstable in the linear inviscid limit when used in baroclinic flows as discretized in [11, 19]. Of interest is that the *barotropically* dissipative backward-time discretization of the barotropic mode is theoretically *baroclinically* dissipation-free and stable for a forward-time discretization of the baroclinic mode. We further demonstrate that in practice, the backward-time barotropic discretization with a forward-time baroclinic discretization in a TRIM method is only baroclinically stable over long time scales if the density interpolation to cell faces is (at least) slightly numerically diffusive. That is, use of non-diffusive second-order spatial interpolation for density transport leads to a practical amplification factors that are very slightly greater than unity instead of exactly unity. This result is still consistent with our stability analysis as the latter does not include the density centre/face interpolation that is necessary for the TRIM solution. As these results indicate some significant drawbacks to the existing TRIM method, we examine the theoretical characteristics of a family of 2-level, 2-step predictor-corrector schemes that may be more suitable for future model development.

The following presents: (Section 2) the general methodology for the stability analysis numerical schemes, followed by (Section 3) results and discussion of the stability analysis, practical stability of the TRIM method, and theoretical stability for a new predictor-corrector method, and finally (Section 4), a summary of conclusions that can be drawn from this work.

2. METHODOLOGY

Our general approach is to provide a linear stability analysis of the baroclinic mode in a 2-level, single-step TRIM method that is used for SWE simulations. We examine the linkage between the baroclinic stability analysis and the SWE implementation in a baroclinic/barotropic solution. We demonstrate that SWE simulations using the TRIM scheme with linearized momentum have the

DOI: 10.1002/fld

general stability characteristics predicted by the stability analysis. For simplicity in exposition while retaining necessary local and global conservation properties in the numerical method, we neglect nonlinear momentum terms while retaining nonlinearity in both barotropic/baroclinic coupling and conservative transport of scalars (which are otherwise neglected in the stability analysis). Our approach cannot prove absolute stability for a nonlinear implementation, but it demonstrates the linear stability limits in both a theoretical and practical manner.

2.1. Governing equations

We are interested in establishing numerical stability in the linear inviscid limit, so we begin with the incompressible, hydrostatic Euler equations with the Boussinesq approximation. For baroclinic flows, numerical stability in the inviscid limit is a desirable property as stratification can suppress turbulence, therefore, limiting turbulent vertical viscosity/diffusivity to near-molecular levels.

The governing equations considered for linear stability analysis in this work are

$$\frac{\partial u}{\partial x} + \frac{\partial w}{\partial z} = 0 \tag{1}$$

$$\frac{\partial u}{\partial t} + \frac{1}{\rho}\frac{\partial p}{\partial x} = 0 \tag{2}$$

$$\frac{\partial p}{\partial z} + g\rho = 0 \tag{3}$$

$$\frac{\partial \rho}{\partial t} + \frac{\partial \rho u}{\partial x} + \frac{\partial \rho w}{\partial z} = 0 \tag{4}$$

where u and w are the velocity components in the x and z directions, g is gravity, ρ is water density, and p is the pressure. The transport of density in Equation (4) is the equivalent of transporting an active scalar (e.g. temperature, salinity) with a linear equation of state. The 2D x–z equations are used, rather than the full 3D equations as the fundamental stability issues for baroclinic flows (without Coriolis) are inherently determined by basic horizontal/vertical motions of internal waves.

Equations (1)–(4) are inviscid and linear for momentum, which is consistent with: (1) a time-invariant background density distribution (i.e. no turbulent mixing or viscous diffusion) and (2) small-amplitude oscillations. This linearized model, when coupled with further linearization of density transport, the hydrostatic and Boussinesq approximations, and neglect of barotropic/baroclinic coupling, admits an analytical solution useful for model verification (discussed in [23]).

2.2. The semi-implicit, baroclinic forward-time solution of inviscid SWE

The TRIM method outlined in [1] and succeeding papers applies implicit solution of integrated continuity based on a θ-weighting that can be adjusted to create a centred-time discretization using $\theta = \frac{1}{2}$ or a backward-time discretization using $\theta = 1$. For any $\theta < \frac{1}{2}$ the TRIM method is barotropically unstable. Discretization of the baroclinic term in the TRIM method [11] is forward-time so that density transport is computationally decoupled from both momentum and continuity. The TRIM approach, a semi-implicit, baroclinic forward-time method, is briefly described here for the sake of clarity. The linkage between TRIM-style SWE models and the simplified methods adopted in the stability analysis is presented below, referring to concepts introduced here.

DOI: 10.1002/fld

In the 3D SWE for density-stratified flows with a free surface, the pressure gradient may be separated into its barotropic and baroclinic parts, i.e.

$$\frac{\partial p}{\partial x} = g\rho_0 \frac{\partial \eta}{\partial x} + g \int_z^\eta \frac{\partial}{\partial x}\{\overline{\rho}(z) + \rho'\}\, \mathrm{d}z \tag{5}$$

This equation is obtained by integrating in depth and differencing the hydrostatic equation (3). Here, η is the free surface displacement from equilibrium and the density $\rho(x, z)$ has been decomposed as $\rho(x, z) = \rho_0 + \overline{\rho}(z) + \rho'(x, z)$, where ρ_0 is the reference density and ρ' is the density perturbation from the background (at rest) density profile $\overline{\rho}(z)$. Introducing Equation (5) and the Boussinesq approximation in Equation (2) provides the linearized horizontal momentum equation as

$$\frac{\partial u}{\partial t} + g\frac{\partial \eta}{\partial x} + \frac{g}{\rho_0}\int_{z'}^{\eta} \frac{\partial \rho}{\partial x}\, \mathrm{d}z = 0 \tag{6}$$

where the $\overline{\rho} + \rho'$ notation (required for linear baroclinic equations, Section 2.3) may be conveniently replaced with ρ without loss of generality. Solution of the hydrostatic equations requires an additional equation for the free surface, which is obtained in the standard fashion by integrating the continuity, Equation (1) over the water column and applying the kinematic boundary condition at the free surface (e.g. [24]), resulting in

$$\frac{\partial \eta}{\partial t} + \frac{\partial}{\partial x}\int_{-H}^{\eta} u\, \mathrm{d}z = 0 \tag{7}$$

Here, $z = -H(x)$ is the depth of the bottom boundary measured from the undisturbed free surface $z = 0$. No flux of water or temperature is allowed through the bottom or the free surface (imposed boundary conditions).

Equations (1), (4), (6) and (7) are a closed set for numerical solution of u, w, ρ, and η and are an inviscid 2D form of the more general SWE. The 'θ-method' proposed by Casulli and Cattani [10] is adopted herein. The method can be presented for a Cartesian Arakawa C (staggered) grid as

$$u_{i+1/2,k}^{n+1} = u_{i+1/2,k}^{n} - g(1-\theta)\frac{\Delta t}{\Delta x}(\eta_{i+1}^{n} - \eta_i^{n}) - g\theta\frac{\Delta t}{\Delta x}(\eta_{i+1}^{n+1} - \eta_i^{n+1}) - \frac{\Delta t}{\Delta x}\frac{g}{\rho_0}\sum_{m=k}^{k_{\max}}(\rho_{i+1,m}^{n} - \rho_{i,m}^{n})\Delta z_{i+1/2,m}^{n} \tag{8}$$

$$\eta_i^{n+1} = \eta_i^{n} - \frac{\Delta t}{\Delta x}\left(\sum_{k=1}^{k_{\max}} F_{i+1/2,k}^{n+\theta} - \sum_{k=1}^{k_{\max}} F_{i-1/2,k}^{n+\theta}\right) \tag{9}$$

$$G_{i,k+1/2}^{n+\theta} = G_{i,k-1/2}^{n+\theta} - F_{i+1/2,k}^{n+\theta} + F_{i-1/2,k}^{n+\theta} \tag{10}$$

$$\rho_{i,k}^{n+1}\Delta z_{i,k}^{n+1} = \rho_{i,k}^{n}\Delta z_{i,k}^{n} - \frac{\Delta t}{\Delta x}(\rho_{i+1/2,k}^{n+1/2} F_{i+1/2,k}^{n+\theta} - \rho_{i-1/2,k}^{n+1/2} F_{i-1/2,k}^{n+\theta}) - \frac{\Delta t}{\Delta x}(\rho_{i,k+1/2}^{n+1/2} G_{i,k+1/2}^{n+\theta} - \rho_{i,k-1/2}^{n+1/2} G_{i,k-1/2}^{n+\theta}) \tag{11}$$

DOI: 10.1002/fld

where F and G are horizontal and vertical fluxes (further defined below), and the solution is over vertical layers numbered $k = 1 \ldots k_{\max}$. Here, Δz is the vertical dimension (thickness) of the computational cells. Changes in free surface elevation are incorporated by changing the thickness of the top-most computational cells, $\Delta z_{i,\,k_{\max}}$ (see [1] for example), according to

$$\Delta z^n_{i,\,k_{\max}} = \Delta z^0_{k_{\max}} + \eta^n_i$$

where $\Delta z^0_{k_{\max}}$ is a nominal time-invariant thickness for the top-most grid cells. In the most general case, $\Delta z^0_{k_{\max}}$ will be different from the fixed time-invariant thickness for other subsurface cells. This definition of cell thickness, in strict temporal agreement with the definition of the dynamic-free surface elevation, contrasts with the definition used in the NLFS method of Campin *et al*. [7] in which Δz and η are allowed to lag in time. However, it can be noted that in the standard TRIM formulation of Equation (8), the discretization of the baroclinic term has $\Delta z^n_{i,\,k_{\max}}$ that is lagged from the free surface discretization η^{n+1}_i. For the present work, the free surface does not have significant motion so there is no need for wetting/drying of computational cells as developed in the TRIM models.

Equation (8) is the linearized momentum equation with the θ-method for the barotropic term and forward-time discretization of the baroclinic term. In Equation (9), the discrete approximation of the horizontal volume flux rate from time 'n' to time '$n+1$' on cell face $i+\frac{1}{2}$ is defined as a combination of the time 'n' and '$n+1$' velocities as

$$F^{n+\theta}_{i+1/2,\,k} \equiv (1-\theta)u^n_{i+1/2}\Delta z^{n-1}_{i+1/2,\,k} + \theta u^{n+1}_{i+1/2}\Delta z^n_{i+1/2,\,k} \tag{12}$$

where θ is the same weighting parameter applied in momentum, Equation (8). Note that the use of Δz^{n-1} in this flux discretization is a subtlety that has been neglected in the literature (see Appendix A). The vertical flux, $G^{n+\theta}$, over the time step and across the $k \pm \frac{1}{2}$ faces of all but the top-most grid cells is obtained from Equation (10), which diagnostically enforces local continuity, Equation (1), subject to the zero-flux bottom boundary condition $G_{i,\,1/2} = 0$. Note that the method is flux based and does not require explicit computation of a primitive vertical velocity. For the top-most grid cells, local continuity requires that difference between volume fluxes entering in and going out of grid cell must be equal to change of grid cell volume between time steps, i.e.

$$\eta^{n+1}_i - \eta^n_i = (G^{n+\theta}_{i,\,k_{\max}-1/2} - F^{n+\theta}_{i+1/2,\,k_{\max}} + F^{n+\theta}_{i-1/2,\,k_{\max}}) \tag{13}$$

Equation (11) provides a discretization of conservative flux-based density transport, Equation (4), that is consistent with continuity [25]. The density $\rho^{n+1/2}_{i+1/2,\,k}$ is the density at the '$i+\frac{1}{2}$' cell face that is appropriate for time '$n+\frac{1}{2}$'. Herein both central difference and quadratic interpolation using the time 'n' density field are applied.

The numerical solution of the SWE following the general TRIM form of [10] requires substitution of Equation (8) into (12) and then into Equation (9) to provide a banded-diagonal matrix (tridiagonal in 2D) for the free surface position, η^{n+1}. Momentum update is subsequently provided by Equation (8), the vertical flux is diagnostically computed from Equation (10) and density transport is subsequently obtained from Equation (11). In the present model we use a conjugate gradient method for banded matrix solution similar to that proposed in [1, 10].

DOI: 10.1002/fld

2.3. Linear baroclinic equations and the analytical solution

To study the stability and phase propagation errors of the baroclinic discretization of two-level semi-implicit methods, we consider the linear baroclinic equations (e.g. [19]), which are defined in terms of the departure from the depth-averaged velocities for a system with a quiescent-free surface, i.e.

$$u' = u - \frac{1}{H+\eta}\int_{-H}^{\eta} u \, \mathrm{d}z \tag{14}$$

The linear baroclinic equations are derived by subtracting the barotropic equations from the full system of equations (see Appendix B for a detailed analysis), and are given by

$$\frac{\partial u'}{\partial x} + \frac{\partial w'}{\partial z} = 0 \tag{15}$$

$$\frac{\partial u'}{\partial t} + \frac{1}{\rho_0}\frac{\partial p'}{\partial x} = 0 \tag{16}$$

$$\frac{\partial p'}{\partial z} + \rho' g = 0 \tag{17}$$

$$\frac{\partial \rho'}{\partial t} + w' \frac{\partial}{\partial z}\overline{\rho}(z) = 0 \tag{18}$$

where all variables have been previously defined (see Equation (5)). For our purposes, a linear stratification is used as the background, such that

$$\overline{\rho}(z) = -\gamma z \tag{19}$$

where $z = 0$ is the undisturbed free surface (positive z is upwards) and γ is a constant (initial condition). Using a linear stratification simplifies the following analysis.

The governing equations for stability analysis, Equations (15)–(18), are the linear, inviscid, hydrostatic, baroclinic counterpart of the full SWE. The principal difference between a particle numerical solution of the inviscid linearized SWE and the linear baroclinic equations is the neglected linkage to the barotropic term. That is, Equation (16) *a priori* neglects the barotropic/baroclinic coupling, which is a necessary part of a practical SWE model. Furthermore, the linearized equation for the density perturbation requires dropping the term $\partial \rho u / \partial x$ from Equation (4) to obtain Equation (18), i.e. the horizontal fluxes of density are neglected. Note, also, that density transport in the perturbation form, Equation (18), is linear, so the spatial interpolation scheme to get face values from densities defined at cell centres, appearing in Equation (11), is not represented within the stability analysis. The resulting Equations (15)–(18) are, however, consistent with the assumption of small-amplitude oscillations (see Appendix B for a detailed analysis), and identify the stiffest process (propagation of internal waves due to constant stratification).

2.4. Forward-time baroclinic equations

To understand stability of the TRIM method, we develop an equivalent discretization of the linear baroclinic equations, Equations (15)–(18). If $\eta(x, t) \approx 0$ and the baroclinic wave amplitude is small, then the SWE reduce to Equations (15)–(18) so the stability analysis of the latter equations should

DOI: 10.1002/fld

apply to the former. For simplicity, the primes are dropped in the following analysis. The discrete time advance of 'u' and 'ρ' are found from Equations (16) and (18) using second-order spatial differences that can be represented in the semi-discrete form as

$$\frac{\partial}{\partial t} u_{i+1/2,k} + \frac{1}{\rho_0} \frac{p_{i+1,k} - p_{i,k}}{\Delta x} = 0 \tag{20}$$

$$\frac{\partial}{\partial t} \rho_{i,k} + \frac{w_{i,k+1/2} + w_{i,k-1/2}}{2} \frac{\partial \overline{\rho}}{\partial z} = 0 \tag{21}$$

These evolution equations are numerically coupled only through the spatial discretizations of continuity, Equation (15), and the pressure gradient, Equation (17), which can be represented using second-order central differences as

$$\frac{u^*_{i+1/2,k} - u^*_{i-1/2,k}}{\Delta x} + \frac{w^*_{i,k+1/2} - w^*_{i,k-1/2}}{\Delta z} = 0 \tag{22}$$

$$g \frac{\rho^*_{i,k+1} + \rho^*_{j,k}}{2} + \frac{p^*_{i,k+1} - p^*_{i,k}}{\Delta z} = 0 \tag{23}$$

where the superscript '$*$' indicates any consistent time-level.

To find the fully discrete forms of Equations (20) and (21) that are analogous to the TRIM method, we note that TRIM applies an implicit solution of the barotropic term in momentum (i.e. the θ-method), Equation (8), but uses a forward-time discretization of the baroclinic term. We will call this a *baroclinic forward-time* method as our focus is on the baroclinic term and the barotropic mode is assumed zero in the stability analysis. A baroclinic forward-time discretization of the linear baroclinic horizontal momentum, Equation (20), for an undisturbed free surface is

$$\frac{u^{n+1}_{i+1/2,k} - u^n_{i+1/2,k}}{\Delta t} + \frac{1}{\rho_0} \left[\frac{p^n_{i+1,k} - p^n_{i,k}}{\Delta x} \right] = 0 \tag{24}$$

where the pressure in a purely baroclinic flow is the hydrostatic pressure of the perturbed density field. It follows that Equation (24) is equivalent to Equation (8) for $\eta(x, t) = 0$. Once the horizontal velocity is known from Equation (24), the vertical velocity, w^{n+1}, is computed from Equation (22) where all '$*$' values are at time '$n + 1$', and is a diagnostic solution rather than a time advance. The density transport then follows from the known time 'n' and '$n + 1$' vertical velocities as

$$\frac{\rho^{n+1}_{i,k} - \rho^n_{i,k}}{\Delta t} + \frac{1}{2}[(w^{n+1}_{i,k+1/2} + w^{n+1}_{i,k-1/2})\theta + (w^n_{i,k+1/2} + w^n_{i,k-1/2})(1 - \theta)] \frac{\partial \overline{\rho}}{\partial z} = 0 \tag{25}$$

The θ-weighting is included in Equation (25) to provide a discretization similar to flux weighing, Equation (12), used in the TRIM density transport, Equation (11). Note that Equation (25), does not include the horizontal fluxes of Equation (11), which are removed in the linearization for Equation (18). As a final numerical step, the updated pressure field, p^{n+1}, is computed diagnostically from Equation (23) using time '$n + 1$' data.

Equations (8), (10) and (11) are the semi-implicit baroclinic forward-time discrete equations of the SWE that are functionally equivalent to Equations (24), (22), and (25), respectively, of the baroclinic forward-time method for the linear baroclinic equations. Note that Equation (23) is developed from Equation (3), which becomes a trivial identity for the hydrostatic pressure

DOI: 10.1002/fld

relationship in the SWE solution. Because the equations are functionally equivalent in their discrete forms, the behaviour of a SWE numerical solution for a linear baroclinic wave using the semi-implicit baroclinic forward-time method is, as it will be shown, governed by the stability limits developed for the baroclinic forward-time method below.

Although our focus is on the TRIM method, our stability analysis (below) is also applicable to the NLFS method of [7]. If we introduce θ in Equation (24) as a weighting for the pressure rather than as a weighting for vertical velocity in Equation (25), that is

$$\frac{u_{i+1/2,k}^{n+1} - u_{j=i+1/2,k}^{n}}{\Delta t} + \frac{1}{\rho_0}\left[\frac{(p_{i+1,k}^{n+1} - p_{i,k}^{n+1})\theta + (p_{i+1,k}^{n} - p_{i,k}^{n})(1-\theta)}{\Delta x}\right] = 0 \tag{26}$$

$$\frac{\rho_{i,k}^{n+1} - \rho_{i,k}^{n}}{\Delta t} + \frac{\mathrm{d}\overline{\rho}}{\mathrm{d}z}\left[\frac{w_{i,k+1/2}^{n} + w_{i,k-1/2}^{n}}{2}\right] = 0 \tag{27}$$

then the scalar transport equations are first solved using Equation (27) followed by the solution of the momentum equation (26), with the baroclinic pressure gradient terms calculated from a density field which is obtained by some 'averaging' of the densities at time n and $n+1$. This baroclinic discretization is functionally equivalent to the NLFS method in [7]. Interestingly enough, the characteristic equation (developed below) is unchanged when Equations (26) and (27) are used in place of Equations (24) and (25), so the characteristic equation stability analysis presented in the Results and Discussion section, and the conclusions drawn therein, are also applicable to the baroclinic discretization of the NLFS method. However, we have not directly tested the NLFS method, so stability behaviour in practical implementations remains an open question.

2.5. Stability analysis methods

For baroclinic wave analysis of the numerical discretization, we adopt a Fourier procedure similar to surface gravity wave analysis used by Gray and Lynch [26] and attributed to Leendertse [27]. The general solution to Equations (15)–(18) is represented by a series of 'm' Fourier modes as

$$u' = \sum_m U_0^m \exp(\mathrm{i}\alpha_m x + \mathrm{i}\beta_m z + \mathrm{i}\omega_m t) = \sum_m \hat{u}^m \tag{28}$$

$$w' = \sum_m W_0^m \exp(\mathrm{i}\alpha_m x + \mathrm{i}\beta_m z + \mathrm{i}\omega_m t) = \sum_m \hat{w}^m \tag{29}$$

$$p' = \sum_m P_0^m \exp(\mathrm{i}\alpha_m x + \mathrm{i}\beta_m z + \mathrm{i}\omega_m t) = \sum_m \hat{p}^m \tag{30}$$

$$\rho' = \sum_m \Theta_0^m \exp(\mathrm{i}\alpha_m x + \mathrm{i}\beta_m z + \mathrm{i}\omega_m t) = \sum_m \hat{\rho}^m \tag{31}$$

where ω is the oscillation frequency. The horizontal and vertical wave numbers are α $(=2\pi/\mathtt{l}_x)$ and β $(=2p/\mathtt{l}_z)$, where $\mathtt{l}_x$ and $\mathtt{l}_z$ are the horizontal and vertical wavelengths. For the linear equations, solution of a single mode provides the solution for all modes. Hence, for simplicity, mode superscripts and subscripts are dropped for analysis of a single generic mode.

The relationship between α, β, and ω (dispersion relationship) for Equations (28)–(31) will be valid for all wavelengths. This relationship can be found for the analytical case by substituting a

DOI: 10.1002/fld

single mode of Equations (28)–(31) into Equations (15)–(18), which yields

$$\mathrm{i}\alpha U_0 + \mathrm{i}\beta W_0 = 0 \tag{32}$$

$$\mathrm{i}\omega U_0 + \frac{\mathrm{i}\alpha}{\rho} P_0 = 0 \tag{33}$$

$$\mathrm{i}\beta U_0 + g\Theta_0 = 0 \tag{34}$$

$$\mathrm{i}\omega\Theta_0 + W_0 \frac{\mathrm{d}\overline{\rho}}{\mathrm{d}z} = 0 \tag{35}$$

Eliminating U_0, W_0, Θ_0 and P_0 from these four equations provides the analytical dispersion relation

$$\omega^2 = N^2 \left(\frac{\alpha}{\beta}\right)^2 \tag{36}$$

where N is the constant background Brunt–Väisälä frequency, $N^2 = -(g/\rho_0)(\partial\rho/\partial z)$. This dispersion relation is the limiting hydrostatic case (waves with horizontal wavelengths much longer than their vertical wavelengths) of the more general dispersion relation for non-hydrostatic flows (e.g. [28]).

The ratio of the solution at time $t + \Delta t$ to that at time t is given by $\lambda = \exp(\mathrm{i}\omega\Delta t)$, and is known as the amplification factor. The analytical value of ω, from Equation (36), results in the analytical amplification factor λ_a as

$$\lambda_\mathrm{a} = \exp\left(\mathrm{i}N\frac{\alpha}{\beta}\Delta t\right) = \exp(\mathrm{i}\varphi) \tag{37}$$

where it is convenient to define

$$\varphi = N\frac{\alpha}{\beta}\Delta t \tag{38}$$

Substituting Equations (28)–(31) into the finite difference approximation Equations (22)–(25), provides an algebraic system of equations. The amplification factors for the numerical schemes are the eigenvalues of the matrices for the time advance and they represent the numerical counterpart of Equation (37), i.e.

$$\lambda = \exp(\mathrm{i}\omega_\mathrm{N}\Delta t) = \exp(\mathrm{i}\varphi_\mathrm{N}) \tag{39}$$

The theoretical (λ_a) and discrete (λ) amplification factors are used to characterize the phase and amplitude errors associated with the discretization method (see Section 3). The characteristic equation for the baroclinic forward-time approach can be found (see Appendix C for details) in terms of the amplification factor, λ, as

$$\lambda^2 + (\theta B^2 - 2)\lambda + (1 + B^2[1 - \theta]) = 0 \tag{40}$$

where B is a non-dimensional number, given by

$$B = N\Delta z \frac{\Delta t}{\Delta x} \sin\left(\alpha\frac{\Delta x}{2}\right) \tan^{-1}\left(\beta\frac{\Delta z}{2}\right) \tag{41}$$

DOI: 10.1002/fld

3. RESULTS AND DISCUSSION

3.1. Overview

A necessary condition for the stability of a numerical scheme is that the amplification factor, Equation (39), obeys $|\lambda| \leqslant 1$. Furthermore, an ideal scheme would have low dissipation so that internal waves may be modelled without artificial damping (however, there are some limits; see [29] for a discussion of how numerical dissipation affects numerical diffusion). If $|\lambda| = 1$ then the numerical scheme is both stable and free from numerical dissipation (at the leading truncation error order). Finally, a good numerical scheme will have low phase propagation error so that internal waves propagate at the correct speeds. For the evaluation of phase errors, at a sufficiently fine spatial discretization ($\alpha/\Delta x \ll 1$ and $\beta/\Delta z \ll 1$) it follows from Equation (41) that $B \to \Delta t N \alpha/\beta$, which means that $B \approx \varphi$ from Equation (38). For a given value of φ, the theoretical amplification factor is $\lambda_a = \exp(i\varphi)$ while the numerical values are the complex roots of the characteristic equation for λ, i.e. Equation (40). The phase angle difference between the numerical roots of the characteristic equation (λ) and the theoretical root (λ_a) is the phase error of the method.

In the following, we show the results of the amplitude and phase error from the stability analysis for the baroclinic forward-time method. We then show that the linearized TRIM semi-implicit baroclinic forward-time behaves, in general, in accord with the predictions of stability theory. Finally, we discuss the implications of this work on the development of practical, stable low-dissipation methods for combined baroclinic/barotropic flows.

3.2. Baroclinic forward-time stability

The stability limitations for barotropic flows with the TRIM method were investigated in [10], where θ is used to set the time weighting of the free surface discretization (integrated continuity). The semi-implicit baroclinic forward-time method shown above is the linearized equivalent of adding a forward-Euler time 'n' baroclinic term to the momentum source term in [10], i.e. the approach used in [11, 19]. The θ in our baroclinic forward-time stability analysis, Equation (25), is the same θ as in [10], since consistency with continuity [25] requires that density transport must use the same weighting as the barotropic discretization. Thus, when barotropic motions are negligible, the effect of θ in a baroclinic solution shows up only in the velocity field used for the density transport. Casulli and Cattani [10] demonstrated that $\frac{1}{2} \leqslant \theta \leqslant 1$ is required for stability in the solution of the barotropic mode, so this provides the limiting θ range for our analysis. Furthermore, they demonstrated that $\theta = \frac{1}{2}$ has small barotropic numerical dissipation, whereas $\theta = 1$ is strongly dissipative of barotropic motions. The $\theta = \frac{1}{2}$ scheme is effectively a time-centred (i.e. Crank–Nicolson) barotropic discretization that is nominally second-order in time, while any $\theta > \frac{1}{2}$ is nominally first-order in time. However, as demonstrated in [18], neither scheme reaches its formal accuracy order for unsteady flows unless: (1) a correction is added for an implicit linearization in the free surface *and* (2) a time step that meets the restrictive *barotropic* CFL condition of $c\Delta t/\Delta x < 1$, where c is the barotropic wave speed. Nevertheless, it is clear from the significant dissipation of barotropic waves documented by Casulli and Cattani [10] for large θ, the preferred method for barotropic flows is $\theta = \frac{1}{2}$. It follows that an ideal baroclinic forward-time method should have $\theta = \frac{1}{2}$ so that when linked with a barotropic solution the method would retain low barotropic dissipation.

The stability analysis for the baroclinic forward-time method, Figure 1, shows that the roots of the characteristic equation fall outside the stability range for any $\theta < 1$. The absolute value of the

DOI: 10.1002/fld

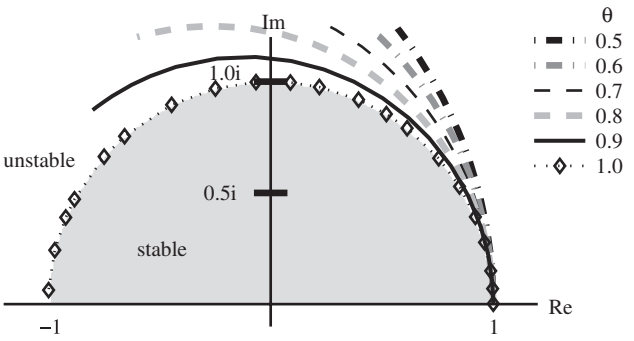

Figure 1. Baroclinic forward-time roots of the characteristic equation (40) for values of $\frac{1}{2} \leqslant \theta \leqslant 1$ that are stable for barotropic flows. Only $\theta = 1$ is conditionally baroclinically stable in the inviscid linear limit.

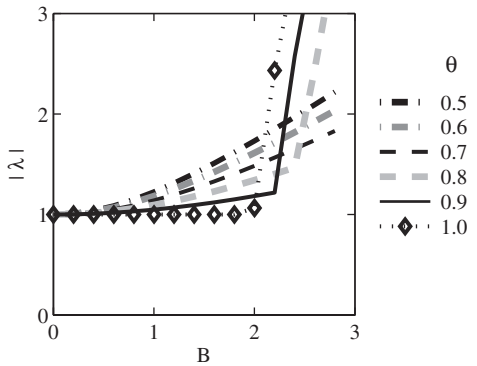

Figure 2. Baroclinic forward-time discrete amplification factor, λ, as a function of the stability characteristic, B, from Equation (41). Note that where there are two values of $|\lambda|$ for one value of B, the larger value governs stability and is therefore shown.

amplification factor, Figure 2, indicates the $\theta = 1$ method is conditionally stable for $B \leqslant 2$, which can be confirmed by substitution into Equation (40). It is interesting to note that the barotropic solution with $\theta = 1$ is known to be extremely dissipative of barotropic wave energy [10]; however, the roots of the characteristic equation for the baroclinic motion with $\theta = 1$ fall on the unit-circle (Figure 1) so that $|\lambda| = 1$ (i.e. non-dissipative results) for a wide range of B. Thus, the same approach that is dissipative of barotropic wave energy is essentially conservative of baroclinic energy. Prior model results with $\theta = 1$, though, have shown substantial dissipation of internal waves over the course of long simulations (e.g. [15, 29, 30]), which is likely due to a combination of (1) topographic effects, (2) long-term erosion of the pycnocline by numerical diffusion, and (3) barotropic/baroclinic interactions that extract energy from the baroclinic mode into the barotropic mode where it is quickly dissipated. The present theoretical stability results for the baroclinic forward-time method are verified with numerical modelling below. Phase error for the baroclinic forward-time method is shown in Figure 3. Although the $\theta = 1$ baroclinic forward-time method is stable for the range $1 < B \leqslant 2$, the phase error dramatically increases in this region and $B < 1$ should be preferred for good phase resolution.

DOI: 10.1002/fld

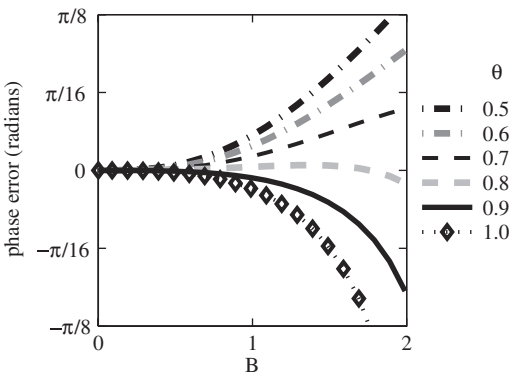

Figure 3. Baroclinic forward-time method phase error for different values of θ. Note that only $\theta = 1$ is stable. Negative values indicate that the numerical wave is slower than the analytical solution (i.e. a lagging phase error).

3.3. Practical stability of the semi-implicit, baroclinic forward-time method

Semi-implicit models with baroclinic forward-time discretizations have been used extensively in both research and engineering applications (see Introduction), so the above finding that the method is inherently unstable for linear inviscid flows with $\theta<1$ deserves further investigation and practical demonstration. A 2D numerical model was written for the present research to solve the inviscid, linear, hydrostatic, Boussinesq, SWE in a rectangular domain on a Cartesian grid. The grid stencil uses a standard Arakawa C grid with velocities on the faces and density at the cell centres. The governing equations are discretized in a flux-conservative manner based on Equations (8)–(11). As the stability analysis method does not limit the choice of face interpolation for the cell-centred densities to the cell faces for the fluxes in Equation (11), the model was developed to use either a centred-difference (CD) approximation or a quadratic upstream approximation (QUICK [31]) at the selection of the user. Note that the model uses linearized momentum, so the comparison of CD *vs* QUICK is simply for the density interpolation. Results reported below investigate both interpolation schemes. A few model runs were conducted with first-order upwind interpolation; however, such results are not reported herein as simple upwinding is so diffusive of the density structure that the internal wave behaviour is hopelessly compromised.

The model was applied to the problem of a linear internal seiche in an enclosed, rectangular, flat-bottom basin with a background linear density profile, which has an analytical solution documented by Eliason and Bourgeois [23] and others. The initial condition for the density field is given by

$$\rho(x, z) = \rho_s - (D - z)\frac{\partial \overline{\rho}}{\partial z} + a\cos\left(\frac{\pi x}{L}\right)\sin\left(\frac{\pi z}{D}\right) \tag{42}$$

where the parameters for the model initial conditions are provided in Table I. The model conditions are for a small-amplitude linear wave so that model conditions are consistent with the linearization of the governing equations in the stability analysis.

The instability of the semi-implicit baroclinic forward-time method for $\theta = \frac{1}{2}$ is illustrated in Figure 4, where the kinetic energy is shown to increase exponentially with time over a wide range of time step sizes. This instability occurs prior to $T/4$ except when a very large number of time

DOI: 10.1002/fld

Table I. Model parameters.

Parameter	Symbol	Value
Basin length	L	28 160 m
Basin depth	D	48 m
Initial density gradient	$\partial\overline{\rho}/\partial z$	-3.64×10^{-2} kg/m^4
Surface density	ρ_s	1025.4 kg/m^3
Initial wave amplitude	a	0.02 m
Brunt–Väisälä frequency	N	1.87×10^{-2} s^{-1}
Basin-scale internal seiche period	T	55 h
Number of wave periods simulated		35
Horizontal grid spacing	Δx	220 m
Vertical grid spacing	Δz	1 m
Time step	Δt	[10, 50, 100, 200 . . . 800] s
Number of horizontal grid cells		128
Number of vertical grid cells		48

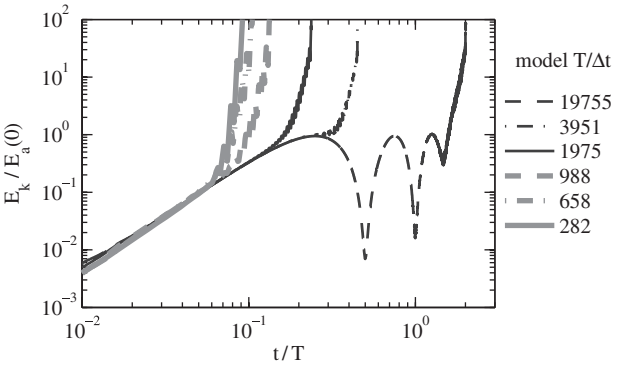

Figure 4. Evolution of kinetic energy, E_k, normalized by initial available potential energy, $E_a(0)$, over three baroclinic seiche wave periods (T) using different time steps (Δt) with $\theta=\frac{1}{2}$ in the forward-time method. Model set-up as in Table I with central difference approximation for density interpolation.

steps were used for each internal wave period (i.e. $T/\Delta t\sim2\times10^4$ for which the instability occurs at approximately $1.3T$). The instability is due to an amplification that scales with the time step, so smaller time steps take longer to reach catastrophically unstable conditions. Animations of the density field (not shown for brevity) indicate the instability begins as grid-scale oscillations in the density field. For small time steps, these oscillations remain small for longer time, but eventually grow to the entire depth of the water column. Additional experiments (not shown) conducted with $\theta=0.9$ and with QUICK in place of central differencing for density interpolation had qualitatively similar results, but with slightly different instability onset.

In contrast to the unstable $\theta=\frac{1}{2}$ results, the energy evolution for $\theta=1$ shown in Figure 5 has similar stable behaviours for a wide range of time step sizes, with instability starting rapidly once a threshold is crossed. The results in Figure 5 are for a limited selection of $T/\Delta t$ and only for the

DOI: 10.1002/fld

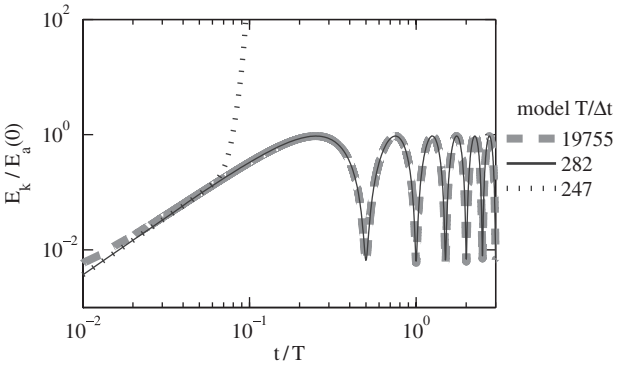

Figure 5. Evolution of kinetic energy, E_k, normalized by initial available potential energy, $E_a(0)$, over three baroclinic seiche wave periods (T) using different time steps (Δt) with $\theta = 1$ in the forward-time method. Model set-up as in Table I with central difference approximation for density interpolation.

central difference density interpolation; however, results for other values of $T/\Delta t > 282$ and results for quadratic upwind interpolation are similar.

To compare the amplitude and phase error of the semi-implicit, baroclinic forward-time numerical method to the predictions of stability theory, it is necessary to define the relationship between B in Equation (41) and the numerical method. Noting that the basin-scale internal seiche frequency is

$$\omega_s = \frac{ND}{L} \tag{43}$$

then the Courant number for the basin-scale internal seiche is

$$C_s = \frac{ND}{\pi}\frac{\Delta t}{\Delta x} \tag{44}$$

The maximum value of B associated with a discrete numerical solution can be estimated using Equation (41) as

$$B_{\max} = \frac{\pi \Delta z}{D} C_s \sin\left(\max[k_x]\frac{\Delta x}{2}\right) \tan^{-1}\left(\min[k_z]\frac{\Delta z}{2}\right) \tag{45}$$

where $\max[k_x]$ is the largest possible horizontal wave number disturbance represented on the model grid, i.e. $k_x = \pi/\Delta x$ for a disturbance of length $2\Delta x$. Similarly, $\min[k_z]$ is the smallest possible vertical wave number disturbance represented on the grid, i.e. $k_z = \pi/D$ for a disturbance of length 2D. Evaluating the sin and tan functions in Equation (45) for $\Delta z \ll D$, it follows that

$$B_{\max} \approx 2C_s \tag{46}$$

Thus, the result that $B < 2$ is generally required for stability of explicit methods is consistent with an outer limit of $C_s < 1$. Note that this stability limit is for a disturbance that begins at the smallest horizontal spatial scale and propagates upscale.

To examine the model results, we analyse the kinetic energy signature, which has a frequency that is twice the basin-scale seiche. Any linear wave will have two kinetic energy peaks in each wave period (i.e. when the isopycnals are flat, all of the wave available potential energy has

DOI: 10.1002/fld

been converted into kinetic energy). The model practical stability must correspond to the peak behaviour—e.g. continually increasing peak kinetic energy values are a sign of an unstable solution. Over the 35 wave periods simulated, an exponential of the form

$$E_{\text{fit}} = c_1 \exp\left(c_2 \frac{t}{T}\right) \tag{47}$$

is fitted to the peak kinetic energy values with typical results shown in Figure 6. The R^2 values for the regression and the root-mean-square (RMS) difference between the exponential fit and the normalized kinetic energy are shown in Table II, indicating good agreement. Note that linear fits would have been just as successful for the present results; however, the exponential fit is consistent with expected behaviour, according to the stability analysis. The model amplification factor for

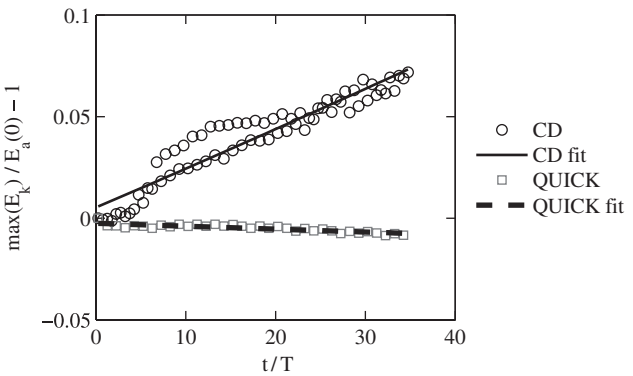

Figure 6. Examples of normalized maximum kinetic energy in each wave period, $\max(E_k)$ and the best-fit line used to compute the amplification factor. Results shown are for $\theta = 1$ and $T/\Delta t = 282$ for central difference (CD) and upwind quadratic (QUICK) approximations of face densities.

Table II. Kinetic energy fit.

	CD		QUICK	
$T/\Delta t$	R^2	RMS	R^2	RMS
282	0.9	6.6×10^{-3}	0.69	8.0×10^{-4}
329	0.86	7.1×10^{-3}	0.67	8.1×10^{-4}
395	0.85	7.0×10^{-3}	0.66	8.1×10^{-4}
494	0.83	7.0×10^{-3}	0.62	8.2×10^{-4}
658	0.80	7.0×10^{-3}	0.56	8.1×10^{-4}
988	0.80	6.8×10^{-3}	0.47	8.2×10^{-4}
1975	0.78	7.0×10^{-3}	0.38	8.9×10^{-4}
3951	0.75	7.2×10^{-3}	0.33	9.6×10^{-4}
19 755	0.76	6.8×10^{-3}	n/a	n/a

DOI: 10.1002/fld

the 'nth' peak is estimated from the fitted exponential line as

$$\lambda_m(n) \approx \frac{E(n)}{E(n-1)} \tag{48}$$

The simulation wave period for the 'nth' peak is computed from

$$T_m(n) = t(n) - t(n-1) \tag{49}$$

where $t(n)$ is the time to the 'nth' peak. For each simulation, the mean wave period computed over 35 wave periods was approximately 1.98×10^5 s, with a maximum standard deviation in any simulation of 290 s. Thus, all simulations have consistent wave periods over the entire the simulation time and can be characterized by the mean period or its inverse, the mean basin-scale seiche frequency.

Using the above approach, the amplification factors for all the $\theta = 1$ simulations for $B_{\max} < 2$ are shown in Figure 7. Note that both central difference and upwind quadratic approximations of the cell-face densities result in $|\lambda| \sim 1$, however, the central difference results show an amplification factor slightly greater than unity while the quadratic upstream is slightly less. All results remained stable for the 35 wave periods simulated. Note that this corresponds to 80 days of simulation for a 30 km long basin, so is of reasonably good stability. However, central difference simulations over longer times (not shown) eventually becomes unstable due to the amplification factor being marginally greater than unity. In contrast, the quadratic upstream difference approach did not show any long time-scale instability, which is consistent with the amplification factor being marginally smaller than unity. Note that for $B_{\max} > 2$, kinetic energy showed exponential increases and therefore large λ for both upwind quadratic and central difference methods. Results for $B_{\max} > 2$ are all unstable and similar to the results for $T/\Delta t = 247$ in Figure 5.

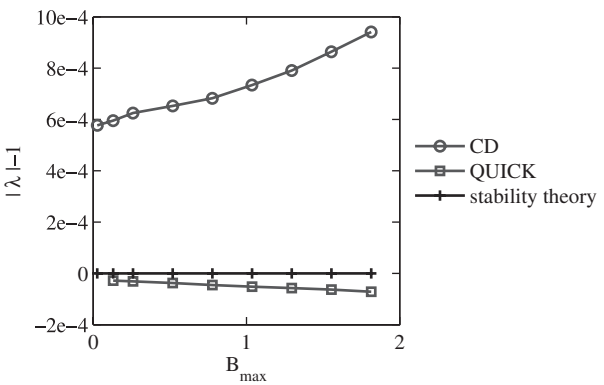

Figure 7. Comparison of stability theory and mean amplification factor for 17 stable simulations of the semi-implicit, baroclinic forward-time numerical method for $\theta = 1$ and varying $B_{\max}$. Amplification factors are small for both methods, but show $\lambda > 1$ for central difference (CD) and $\lambda < 1$ for upwind quadratic (QUICK) difference. Error bars are not shown as maximum standard deviation in λ (computed from 35 wave periods) for any simulation is 2.1e−6.

DOI: 10.1002/fld

3.4. Towards an improved SWE 2-level method

The above analysis shows that the semi-implicit, baroclinic forward time method, as popularized by the 2-level TRIM method, is only baroclinically stable in the inviscid limit for $\theta = 1$, which is undesirable for a barotropic/baroclinic flow due to high barotropic dissipation [10]. One might think of this result as requiring a backward-time discretization in the barotropic term to stabilize the otherwise unstable forward-time discretization of the baroclinic term. This idea leads us to ponder whether a method with better stability characteristics might be developed through a centred-time discretization for the baroclinic term, which might then allow a centred-time discretization for the barotropic term (i.e. $\theta = \frac{1}{2}$). Clearly, if we simply attempt to apply a simple Crank–Nicolson discretization of the baroclinic term in momentum, we will require an implicit coupling of density transport with momentum, an undesirable property. However, an alternative approach that allows an approximate centred-time discretization of the baroclinic term without implicit coupling is to invoke a predictor-corrector scheme. In the following, we show that a baroclinic predictor-corrector method can be made theoretically stable with $\theta = \frac{1}{2}$. As there are a number of possible implementation approaches for a semi-implicit, baroclinic predictor-corrector scheme, the development and testing of such a method remains a subject for future investigation. Our goal in the following analysis is to demonstrate that this is a reasonable line of investigation for future model development.

The general scheme for the proposed baroclinic predictor-corrector method is (1) explicit prediction of a horizontal and vertical velocities from time 'n' data, (2) prediction of density transport from a weighted sum of the predicted velocities and the time 'n' velocities, (3) correction of horizontal velocity with a baroclinic term based on a weighted sum of the predicted density field and the time 'n' density field. To illustrate in more detail, horizontal momentum for a predicted velocity, u^{p}, can be obtained from a baroclinic forward-time discretization as

$$\frac{u^{\mathrm{p}}_{i+1/2,\,k} - u^{n}_{i+1/2,\,k}}{\Delta t} + \frac{p^{n}_{i+1,\,k} - p^{n}_{i,\,k}}{\rho_0 \Delta x} = 0 \tag{50}$$

The predicted vertical velocity, w^{p} is computed from Equation (22) with '$*$' superscripts replaced by 'p'.

Once the predicted velocity field is known, predicted density (ρ^{p}) transport is

$$\frac{\rho^{\mathrm{p}}_{i,\,k} - \rho^{n}_{i,\,k}}{\Delta t} + \frac{1}{2}[(w^{\mathrm{p}}_{i,\,k+1/2} + w^{\mathrm{p}}_{i,\,k-1/2})\theta_{\mathrm{p}} + (w^{n}_{i,\,k+1/2} + w^{n}_{i,\,k-1/2})(1-\theta_{\mathrm{p}})]\frac{\partial \overline{\rho}}{\partial z} = 0 \tag{51}$$

where θ_{p} is a weighting factor which must meet the condition $0 \leqslant \theta_{\mathrm{p}} \leqslant 1$, but otherwise may be independently adjusted to develop a family of possible models. The predicted pressure, p^{p}, is obtained from Equation (23), which is used in a horizontal velocity corrector as

$$\frac{u^{n+1}_{i+1/2,\,k} - u^{n}_{i+1/2,\,k}}{\Delta t} + \frac{(p^{\mathrm{p}}_{j+1,\,k} - p^{\mathrm{p}}_{j,\,k})\theta_{\mathrm{b}} + (p^{n}_{j+1,\,k} - p^{n}_{j,\,k})(1-\theta_{\mathrm{b}})}{\rho_0 \Delta x} = 0 \tag{52}$$

where the weighting factor for the baroclinic term, θ_{b}, must meet the condition $0 \leqslant \theta_{\mathrm{b}} \leqslant 1$ but may otherwise be independently set to provide a family of possible predictor-corrector schemes. Note that for $\theta_{\mathrm{b}} = 0$, the predictor step is irrelevant and the discretization collapses to the simple baroclinic forward-time discretization analysed above. For $\theta_{\mathrm{b}} = \frac{1}{2}$, the baroclinic pressure is centred-time and is nominally second-order accurate. To complete the method, vertical velocity, w^{n+1}, is corrected using Equation (22) again with '$*$' replaced by '$n+1$'. The density transport for ρ^{n+1} is identical to

DOI: 10.1002/fld

Equation (25) of the baroclinic forward-time method, including a θ weighting factor for consistency with continuity. The time $n+1$ pressure is computed from Equation (23) with the time $n+1$ values for density.

The characteristic equation for the baroclinic predictor-corrector method can be derived (following a procedure similar to Appendix C) as

$$\lambda^2 + \{B^2(\theta + \theta_b) - B^4\theta\theta_p\theta_b - 2\}\lambda - B^2(\theta + \theta_b - 1) + B^4\theta_p\theta_b(\theta - 1) + 1 = 0 \tag{53}$$

which has three independent choices for parameters $(\theta, \theta_p, \theta_b)$ and B is given by Equation (41). The coefficient θ is the weighting between time 'n' and '$n+1$' for the momentum and free surface equations (identical to the θ in the semi-implicit, baroclinic forward-time method). The new coefficients in the method are θ_p, a weighting for the predictor equations, and θ_b, the weighting of the baroclinic transport between time 'n' and predicted density fields. For stability, we examine the sets of $(\theta, \theta_p, \theta_b)$ provided in Table III. Note that there is no need to test $\theta < \frac{1}{2}$ since such settings are barotropically unstable and therefore not of interest. Furthermore, any case with $\theta_b = 0$ will reduce to the baroclinic forward-time method (analysed above) since the density predictor has no effect on the velocity update in Equation (52) under such conditions.

Figures 8 and 9 show the roots of the characteristic equation that indicates that all forms of the baroclinic predictor-corrector approach are (at least) conditionally stable, i.e stable for some range of B. This finding is a dramatic contrast to the results for the baroclinic forward-time method in Figure 1, wherein only the $\theta = 1$ case is stable. Of interest is that only the case $[\frac{1}{2}, 0, \frac{1}{2}]$ lies on the unit-circle (see Figure 9) and is thus the only candidate for a model without numerical dissipation in the baroclinic mode. For this choice of parameters, the characteristic equation coincides with that of the baroclinic forward-time method. However, it should be noted that the predictor-corrector method obtains this characteristic equation with a non-dissipative method for the free surface $(\theta = \frac{1}{2})$, whereas the forward-time method requires a dissipative-free surface $(\theta = 1)$. In general,

Table III. Predictor-corrector methods examined for stability.

θ	1	1	1	1	1	1	1/2	1/2	1/2	1/2	1/2	1/2
θ_p	1	1	1/2	1/2	0	0	1	1	1/2	1/2	0	0
θ_b	1	1/2	1	1/2	1	1/2	1	1/2	1	1/2	1	1/2

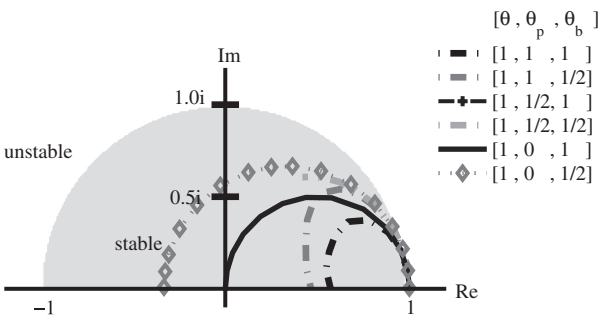

Figure 8. Stable predictor-corrector roots of characteristic equation (53) for $\theta = 1$. For clarity, roots along the real axis (both stable and unstable) have been removed.

DOI: 10.1002/fld

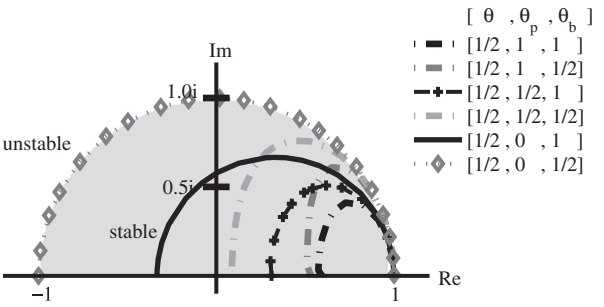

Figure 9. Predictor-corrector roots of characteristic equation (53) for $\theta = \frac{1}{2}$. For clarity, roots along the real axis (both stable and unstable) have been removed.

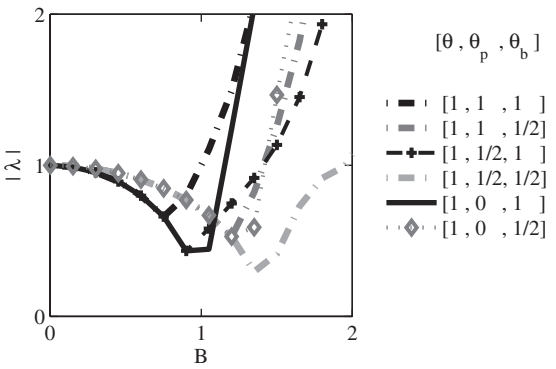

Figure 10. Predictor-corrector discrete amplification factor, λ, as a function of the stability characteristic, B, from Equation (41) for $\theta = 1$.

it appears that the $\theta = \frac{1}{2}$ results (Figure 9) for various θ_p and θ_b are less dissipative (larger $|\lambda|$) than the corresponding cases for $\theta = 1$ (Figure 8). Thus, the baroclinic predictor-corrector scheme has the desired behaviour (compared at baroclinic forward-time) in that $\theta = \frac{1}{2}$ is stable so that a SWE numerical scheme can be designed with minimum barotropic dissipation.

In Figures 10 and 11, the relationship between B and the amplification factor is shown for the baroclinic predictor-corrector method. It can be seen that stability ($|\lambda| \leqslant 1$) requires a lower value of B than associated with the baroclinic forward-time method shown in Figure 2. In Figure 10, with $\theta = 1$, it can be noted that prior to instability, the results fall on two consistent lines, depending on the value of θ_b. For $\theta_b = 1$, the three darker lines are all overlaid until $B \sim 0.7$, and show significantly more dissipation than the lighter lines ($\theta_b = \frac{1}{2}$) that remain overlaid until $B \sim 1.2$. Thus, we conclude that the higher values of θ_b tend to increase baroclinic dissipation and reduce the stability of the method. Indeed, this observation is consistent with the performance in the limit of $\theta_b = 0$, which reduces the baroclinic predictor-corrector to the baroclinic forward-time method (Figure 2) that shows stability for $B \leqslant 2$ and zero dissipation for $\theta = 1$. Also of note, in Figure 10 the case where $\theta_b = \theta_p = \frac{1}{2}$ is stable for $B < 2$, and does not have the rapid development of the instability shown by other schemes.

DOI: 10.1002/fld

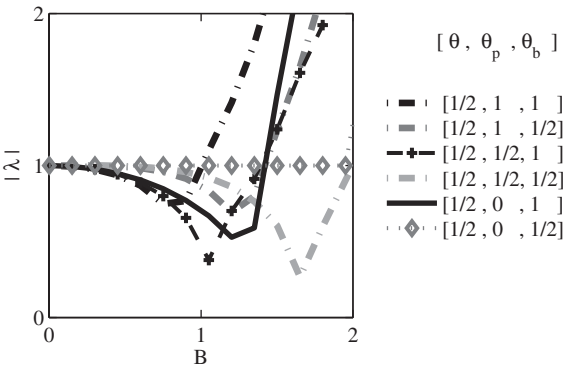

Figure 11. Predictor-corrector discrete amplification factor, λ, as a function of the stability characteristic, B, from Equation (41) for $\theta = \frac{1}{2}$.

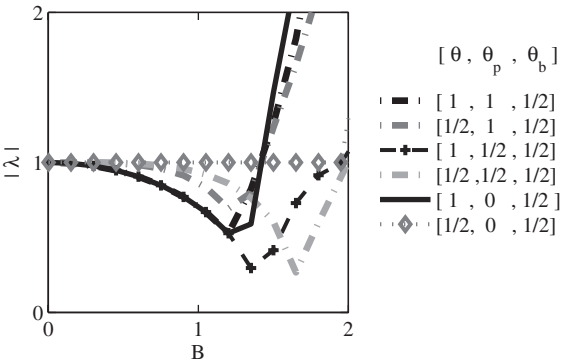

Figure 12. Baroclinic predictor-corrector discrete amplification factor, λ, as a function of the stability characteristic B, from Equation (41) for $\theta_b = \frac{1}{2}$.

Figure 11 has some similarity to Figure 10 in that the results for $\theta_b = 1$ are similar up until $B \sim 0.5$, while results for $\theta_b = \frac{1}{2}$ are similar up until $B \sim 0.7$. Again, we find the $\theta_b = \frac{1}{2}$ case is generally less dissipative and has a higher value of B prior to instability developing. Also similar to Figure 10, the case of $\theta_b = \theta_p = \frac{1}{2}$ remains stable for $B < 2$, without the rapid development of instability seen in other configurations. In Figure 12, a direct comparison of results for $\theta_b = \frac{1}{2}$ confirms that $\theta_p = 1$ shows rapid instability, $\theta_p = \frac{1}{2}$ provides stability out to $B \sim 2$ (albeit with dissipation), and $\theta_p = 0$ provides very different results: dissipative with rapid instability for $\theta = 1$, but dissipationless and stable to $B \sim 2$ for $\theta = \frac{1}{2}$. Clearly, the complexity of the stability behaviour for the baroclinic predictor-corrector method contrasts strongly the behaviour of the baroclinic forward-time method. Indeed, the lesson that the baroclinic forward-time method (stable only for $\theta = 1$) has no applicability to the baroclinic predictor-corrector method, which is unstable at a lower B with $\theta = 1$ than for $\theta = \frac{1}{2}$.

The theoretical phase error of the predictor-corrector method is shown in Figures 13 and 14. It can be seen that the best phase error performance (i.e. over the largest range of B and for

DOI: 10.1002/fld

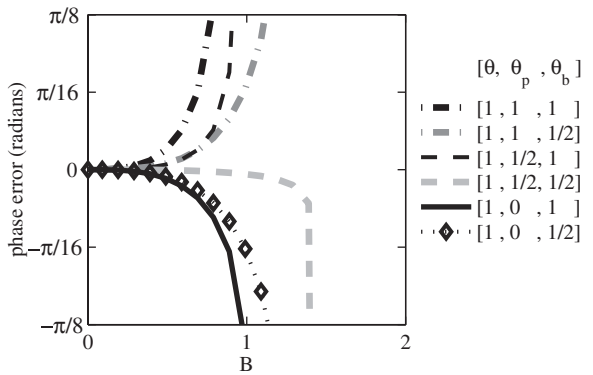

Figure 13. Predictor-corrector method phase error for $\theta = 1$.

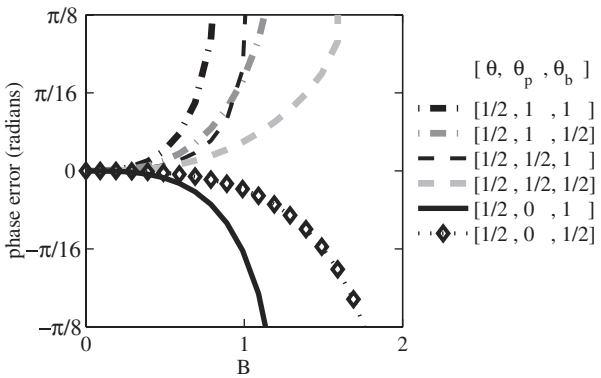

Figure 14. Predictor-corrector method phase error for $\theta = \frac{1}{2}$.

the range of parameter values analysed) is for $[\theta, \theta_p, \theta_b] = [1, \frac{1}{2}, \frac{1}{2}]$. However, it appears that the preferable approaches would be the cases $[\frac{1}{2}, \frac{1}{2}, \frac{1}{2}]$ and $[\frac{1}{2}, 0, \frac{1}{2}]$, which have small phase error for $B < \frac{1}{2}$ along with low dissipation (Figure 11). The theoretical behaviour of alternative $[\theta, \theta_p, \theta_b]$ sets in the predictor-corrector method can be assessed by analysing the form of the numerical amplification factor, which is given by

$$\lambda = \exp \mathrm{i}\varphi \left\{ 1 + \mathrm{i}\,\frac{(\theta_b + \theta - 1)}{2}\,\varphi + \left[\frac{\theta_b + \theta}{2} - \frac{(\theta_b + \theta)^2}{8} - \frac{\theta_b \theta_p}{2} - \frac{1}{3} \right] \varphi^2 \right.$$
$$\left. + \mathrm{i} \left[\frac{(\theta_b + \theta)^2}{4} - \frac{\theta_b + \theta}{2} + \frac{\theta_b \theta_p}{2} - \frac{\theta_b \theta_p \theta}{2} + \frac{1}{4} \right] \varphi^3 + O(\varphi^4) \right\} \tag{54}$$

where φ is given by Equation (38). The above expression can be derived by substituting

$$\lambda = \exp \mathrm{i}\varphi [1 + a\varphi + b\varphi^2 + c\varphi^3 + O(\varphi^4)] \tag{55}$$

DOI: 10.1002/fld

into the characteristic equation, expanding the result in Taylor series for small φ, and setting to zero the resulting polynomial coefficients. It is presumed here that a sufficiently fine spatial resolution is used. The coefficient a will be zero if the condition $\theta+\theta_b=1$ is satisfied. For $[\theta, \theta_p, \theta_b]$, such that $\theta+\theta_b=1$, the predictor-corrector scheme provides a second-order approximation of $\lambda_a=\exp[i\varphi]$. For $\theta+\theta_b<1$, the method is unstable as $|\lambda|>1$. For $\theta+\theta_b>1$, the method becomes dissipative, with dissipation levels increasing for larger $\theta+\theta_b$. A necessary condition for the method to be neutrally stable is a requirement that

$$\theta+\theta_b=1 \tag{56}$$

To be dissipationless a second requirement is $c=0$, which when combined with Equation (56) becomes

$$\theta_b\theta_p(1-\theta)=0 \tag{57}$$

The conditions of Equations (56) and (57) can also be derived from characteristic equation (54). If the zero-order polynomial coefficient in Equation (54) is unity, then the roots appear as a complex conjugate pair whose product is unity. It follows that their absolute values are both unity and the method is neutrally stable.

As shown in [3], slightly dissipative, phase-accurate algorithms can be designed from the analysis of the numerical amplification factor. Using a slightly dissipative baroclinic method may be desirable in a nonlinear hydrostatic model to prevent artificial steepening of internal waves [29]. For the baroclinic predictor-corrector method, dissipation can be enforced by requiring $a=0$ and $b=0$ in Equation (55), while requiring $c\neq 0$. The numerical amplification factor for $\theta+\theta_b=1$ ($a=0$) is given by

$$\lambda=\exp i\varphi\left(1+\frac{\theta_b\theta_p-1/12}{2}\varphi^2+O(\varphi^3)\right) \tag{58}$$

Hence, if $\theta_p\theta_b=\frac{1}{12}$, the algorithm becomes third-order accurate with a dissipative leading order truncation term. For example, for $[\theta, \theta_b]=[\frac{1}{2}, \frac{1}{2}]$, the choice $\theta_p=\frac{1}{6}$ yields the most phase-accurate algorithm. For $\theta_p\theta_b<\frac{1}{12}$ the method would exhibit a positive dispersion (i.e. a faster wave as the baroclinic forward-time method), while for $\theta_p\theta_b>\frac{1}{12}$ result would be a negative dispersion. The choice $[\theta_b, \theta]=[0, 1]$ provides a behaviour equivalent to that of the baroclinic forward-time method, but has a dispersive leading order truncation term.

4. CONCLUSIONS

From the analysis of the semi-implicit, baroclinic forward-time method, we can draw three principal observations. First, and most important, any mass-conservative, two-level, single step, semi-implicit, baroclinic forward-time model of the SWE with $\theta<1$ will be linearly unstable (in the inviscid limit) to small perturbations of the density field. However, from successful prior results in the literature we speculate that this method may be stabilized directly by the addition of viscous (diffusive) terms or indirectly through truncation error in discretizations. Secondly, applying a $\theta=1$ semi-implicit solution to the SWE is stable in the inviscid limit, but as a practical matter may show long-time instability if central differences are used for cell-face density interpolation.

DOI: 10.1002/fld

Using upwind quadratic interpolation for cell-face densities is slightly dissipative and so prevents long-time-scale instability. The implication of this work is that the preferred configuration for non-dissipative simulation of barotropic flows ($\theta = \frac{1}{2}$) is inherently unstable for baroclinic flows, whereas the stable method for baroclinic flows ($\theta = 1$) has previously been shown [10] to be highly dissipative for barotropic flows.

As a possible approach to obtaining a stable method with acceptably small dissipation for both barotropic and baroclinic flows, we examined the stability of a family of proposed 2-level baroclinic predictor-corrector schemes. This family uses separate weightings for momentum continuity (θ), predictor continuity (θ_p) and the baroclinic term (θ_b). Selection of different values for (θ, θ_p, θ_b) provides methods with different stability characteristics. The new approach is shown to be conditionally stable for $\theta = \frac{1}{2}$, which should allow development of a model that is stable for both barotropic and baroclinic modes that does not have the barotropic dissipation caused by using the baroclinic forward-time method at $\theta = 1$. Development and testing of this method is provided in [32].

APPENDIX A: CONSISTENCY IN FLUX DISCRETIZATION

If Equation (12) is substituted into Equation (9), the discretization of depth-integrated continuity, Equation (7) becomes

$$\eta_i^{n+1} = \eta_i^n - (1-\theta)\frac{\Delta t}{\Delta x}\left(\sum_k u_{i+1/2}^n \Delta z_{i+1/2,k}^{n-1} - \sum_k u_{i-1/2}^n \Delta z_{i-1/2,k}^{n-1}\right) - \theta\frac{\Delta t}{\Delta x}\left(\sum_k u_{i+1/2}^{n+1} \Delta z_{i+1/2,k}^{n} - \sum_k u_{i-1/2}^{n+1} \Delta z_{i-1/2,k}^{n}\right) \tag{A1}$$

Note that the above is slightly different than prior formulations in the literature in that the time '$n-1$' values instead of the time 'n' values for Δz are used in the discretization of the time 'n' barotropic term. This approach provides a more consistent definition of the velocity field, as shown below.

Consistent with Equation (12), the relationship between the vertical flux (G) and the primitive velocity (w) is given by

$$G_{i,k+1/2}^{n+\theta} \equiv \Delta x\{(1-\theta)w_{i,k+1/2}^n + \theta w_{i,k+1/2}^{n+1}\} \tag{A2}$$

Local continuity, Equation (10), with substitutions for flux definitions from Equations (12) and (A2), provides (without simplification)

$$w_{i,k+1/2}^{n+1} = w_{i,k-1/2}^{n+1} - \frac{1}{\Delta x}(u_{i+1/2,k}^{n+1}\Delta z_{i+1/2,k}^n - u_{i-1/2,k}^{n+1}\Delta z_{i+1/2,k}^n) - \left(\frac{1-\theta}{\theta}\right) \times \left\{w_{i,k+1/2}^n - w_{i,k-1/2}^n + \frac{1}{\Delta x}(u_{i+1/2,k}^n \Delta z_{i+1/2,k}^{n-1} - u_{i-1/2,k}^n \Delta z_{i-1/2,k}^{n-1})\right\} \tag{A3}$$

DOI: 10.1002/fld

The initial conditions are thus required to meet the condition that

$$w^0_{i,k+1/2} - w^0_{i,k-1/2} + \frac{1}{\Delta x}\left(u^0_{i+1/2,k}\Delta z^{(-1)}_{i+1/2,k} - u^0_{i-1/2,k}\Delta z^{(-1)}_{i-1/2,k}\right) = 0 \tag{A4}$$

where $\Delta z^{(-1)}$ is the grid cell height in the time step before the start of the simulation. If this condition is met, then the bracketed term in Equation (A3) will vanish at all times and the vertical velocity is simply

$$w^{n+1}_{i,k+1/2} = w^{n+1}_{i,k-1/2} - \frac{1}{\Delta x}\left(u^{n+1}_{i+1/2,k}\Delta z^{n}_{i+1/2,k} - u^{n+1}_{i-1/2,k}\Delta z^{n}_{i+1/2,k}\right) \tag{A5}$$

which is a simple discretization of continuity, Equation (1), with a time-lagged vertical grid spacing. Thus, the above approach guarantees that the vertical velocity and the horizontal velocity will always locally satisfy continuity with a time-step-lagged vertical grid size. Note that Equation (A5) must also hold for any 'n' time step as follows:

$$w^{n}_{i,k+1/2} = w^{n}_{i,k-1/2} - \frac{1}{\Delta x}\left(u^{n}_{i+1/2,k}\Delta z^{n-1}_{i+1/2,k} - u^{n}_{i-1/2,k}\Delta z^{n-1}_{i+1/2,k}\right) \tag{A6}$$

So if Δz^n is used in place of Δz^{n-1} in Equation (A1), this is equivalent to doing the same to Equation (A3). It follows that Equation (A5) will not generally hold since it would also require

$$w^{n}_{i,k+1/2} = w^{n}_{i,k-1/2} - \frac{1}{\Delta x}\left(u^{n}_{i+1/2,k}\Delta z^{n}_{i+1/2,k} - u^{n}_{i-1/2,k}\Delta z^{n}_{i+1/2,k}\right) \tag{A7}$$

which cannot be simultaneously true with Equation (A6) for non-trivial flow fields. It follows that u^n in Equation (12) must be multiplied by Δz^{n-1} for consistent enforcement of continuity.

APPENDIX B: DERIVATION OF THE MODEL EQUATIONS

The dynamics of an inviscid fluid in a 2D domain (without Coriolis) may be described by the momentum equations with the Boussinesq approximation (i.e. density is assumed constant in all terms except in the gravitational term),

$$\frac{\partial u}{\partial t} + u\frac{\partial u}{\partial x} + w\frac{\partial u}{\partial z} = -\frac{1}{\rho_0}\frac{\partial p}{\partial x} \tag{B1}$$

$$\frac{\partial w}{\partial t} + u\frac{\partial w}{\partial x} + w\frac{\partial w}{\partial z} = -\frac{1}{\rho_0}\frac{\partial p}{\partial z} - \frac{\rho g}{\rho_0} \tag{B2}$$

and the conservation of mass (continuity),

$$\frac{\partial \rho}{\partial t} + \frac{\partial(\rho u)}{\partial x} + \frac{\partial(\rho w)}{\partial z} = \frac{\partial \rho}{\partial t} + \rho\left(\frac{\partial u}{\partial x} + \frac{\partial w}{\partial z}\right) + u\frac{\partial \rho}{\partial x} + w\frac{\partial \rho}{\partial z} = 0 \tag{B3}$$

We non-dimensionalize Equations (B1)–(B3) by introducing the characteristic scales L, H, c, U and the reference density ρ_0 at the free surface, and two dimensionless parameters ε, γ. The

DOI: 10.1002/fld

resulting non-dimensional variables are as follows:

$$(x, y, z) = L(x^*, y^*, \varepsilon z^*)$$

$$\varepsilon = \frac{H}{L} \ll 1$$

$$c = \sqrt{gH}$$

$$\gamma = \frac{U}{c} \ll 1$$

$$t = \frac{L}{c}\, t^*$$

$$(u, v, w) = \gamma c(u^*, v^*, \varepsilon w^*)$$

$$\rho = \rho_0 \rho^*$$

$$p = \rho_0 c^2 p^*$$

Introducing above scales into Equations (B1)–(B3), rearranging and dropping *, provides

$$\gamma \frac{\partial u}{\partial t} + \gamma^2 \left(u \frac{\partial u}{\partial x} + w \frac{\partial u}{\partial z} \right) = -\frac{\partial p}{\partial x} \tag{B4}$$

$$\gamma \varepsilon^2 \frac{\partial w}{\partial t} + \gamma^2 \varepsilon^2 \left(u \frac{\partial w}{\partial x} + w \frac{\partial w}{\partial z} \right) = -\frac{\partial p}{\partial z} - \rho \tag{B5}$$

$$\frac{\partial \rho}{\partial t} + \gamma \rho \left(\frac{\partial u}{\partial x} + \frac{\partial w}{\partial z} \right) + \gamma \left(u \frac{\partial \rho}{\partial x} + w \frac{\partial \rho}{\partial z} \right) = 0 \tag{B6}$$

For incompressible flow the second term in Equation (B6) evaluates as

$$\gamma \rho \left(\frac{\partial u}{\partial x} + \frac{\partial w}{\partial z} \right) = 0 \tag{B7}$$

So Equation (B6) reduces to

$$\frac{\partial \rho}{\partial t} + \gamma \left(u \frac{\partial \rho}{\partial x} + w \frac{\partial \rho}{\partial z} \right) = 0 \tag{B8}$$

Comparing the governing equations (1)–(4), against Equations (B4), (B5), (B7), and (B8), it can be seen that the former are an $O(\gamma^2 + \gamma\varepsilon^2)$ approximation of the latter. However, Equation (4), is nonlinear and must be further linearized in the stability analysis, as shown in Equation (18). Nevertheless, we can demonstrate that the linear equations for the stability analysis are an approximation of the nonlinear equations with a truncation error of $O(\gamma^2)$. We introduce a regular perturbation expansion with small parameters α and β whose magnitudes relative to ε and γ are to

DOI: 10.1002/fld

be determined [33]

$$u = u_0 + \alpha u_1 + O(\alpha^2) \tag{B9}$$

$$w = w_0 + \alpha w_1 + O(\alpha^2) \tag{B10}$$

$$p = p_0 + \beta p_1 + O(\beta^2) \tag{B11}$$

$$\rho = \rho_0 + \beta \rho_1 + O(\beta^2) \tag{B12}$$

Substituting Equations (B9)–(B12) into Equations (B4), (B5), (B7), and (B8) provides

$$\frac{\partial p_0}{\partial x} + \gamma \frac{\partial u_0}{\partial t} + \beta \frac{\partial p_1}{\partial x} + O(\gamma^2) = 0 \tag{B13}$$

$$\frac{\partial p_0}{\partial z} + \rho_0 + \beta \left(\frac{\partial p_1}{\partial z} + \rho_1 \right) + O(\beta^2) = 0 \tag{B14}$$

$$\gamma \left(\frac{\partial u_0}{\partial x} + \frac{\partial w_0}{\partial z} \right) + O(\gamma\alpha) = 0 \tag{B15}$$

$$\frac{\partial \rho_0}{\partial t} + \beta \frac{\partial \rho_1}{\partial t} + \gamma \left(u_0 \frac{\partial \rho_0}{\partial x} + w_0 \frac{\partial \rho_0}{\partial z} \right) + O(\gamma\alpha) = 0 \tag{B16}$$

We require $O(\beta) = O(\alpha) = O(\gamma) \geqslant O(\varepsilon^2)$, which allows Equations (B13)–(B16) to be written as

$$\frac{\partial p_0}{\partial x} + \gamma \left(\frac{\partial u_0}{\partial t} + \frac{\partial p_1}{\partial x} \right) + O(\gamma^2) = 0 \tag{B17}$$

$$\frac{\partial p_0}{\partial z} + \rho_0 + \gamma \left(\frac{\partial p_1}{\partial z} + \rho_1 \right) + O(\gamma^2) = 0 \tag{B18}$$

$$\gamma \left(\frac{\partial u_0}{\partial x} + \frac{\partial w_0}{\partial z} \right) + O(\gamma^2) = 0 \tag{B19}$$

$$\frac{\partial \rho_0}{\partial t} + \gamma \left(\frac{\partial \rho_1}{\partial t} + u_0 \frac{\partial \rho_0}{\partial x} + w_0 \frac{\partial \rho_0}{\partial z} \right) + O(\gamma^2) = 0 \tag{B20}$$

To obtain the approximation

$$(u, w, p, \rho) = (u_0, \ w_0, \ \ p_0 + \gamma p_1, \ \ \rho_0 + \gamma \rho_1) + O(\gamma^2) \tag{B21}$$

to the desired order, $O(\gamma^2)$, it is necessary that terms of similar order must cancel. It follows that $O(1)$ terms must satisfy

$$\frac{\partial p_0}{\partial x} = 0 \tag{B22}$$

$$\frac{\partial p_0}{\partial z} + \rho_0 = 0 \tag{B23}$$

DOI: 10.1002/fld

$$\frac{\partial \rho_0}{\partial t} = 0 \tag{B24}$$

Similarly, the $O(\gamma)$ terms must satisfy

$$\frac{\partial u_0}{\partial t} + \frac{\partial p_1}{\partial x} = 0 \tag{B25}$$

$$\frac{\partial p_1}{\partial z} + \rho_1 = 0 \tag{B26}$$

$$\frac{\partial u_0}{\partial x} + \frac{\partial w_0}{\partial z} = 0 \tag{B27}$$

$$\frac{\partial \rho_1}{\partial t} + u_0 \frac{\partial \rho_0}{\partial x} + w_0 \frac{\partial \rho_0}{\partial z} = 0 \tag{B28}$$

Equations (B22)–(B24) imply that $\rho_0 = \rho_0(z)$ and $p_0 = p_0(z)$, so that Equation (B28) can be written as

$$\frac{\partial \rho_1}{\partial t} + w_0 \frac{\partial \rho_0}{\partial z} = 0 \tag{B29}$$

Thus, the solution to Equations (B25)–(B27) and (B29) are an $O(\gamma^2)$ approximation of Equations (B1)–(B3). As shown by Camassa and Holm [33], the following equations:

$$u' = \gamma c u_0^*$$

$$w = \gamma c \varepsilon w_0^*$$

$$\overline{p} = \rho_0 c^2 p_0^*$$

$$p' = \rho_0 c^2 \gamma p_1^*$$

$$\overline{\rho} = \rho_0 \rho_0^*$$

$$\rho' = \rho_0 \gamma \rho_1^*$$

are correct to $O(\gamma^2)$. Substituting those equations into Equations (B25)–(B27) and (B29) we obtain dimensional equations that are identical to Equations (15)–(18) used in the linear stability analysis. It follows that the solution set of $(u', w', \overline{p} + p', \overline{\rho} + \rho')$ for Equations (15)–(18) is an $O(\gamma^2)$ approximation of the solution to the governing equations (1)–(4).

APPENDIX C: CHARACTERISTIC EQUATION FOR BAROCLINIC FORWARD-TIME METHOD

Considering the governing equations (15)–(18), we substitute one term 'm' of the general modal solution, Equations (28)–(31), into the discrete equations (22)–(25). Only one term is necessary since the discrete equations are linear and the behaviour of each term of the series is the same as

DOI: 10.1002/fld

the series itself. The result of the substitution is

$$\frac{U_0^m}{\Delta x}\{e^{i\alpha_m(x+\frac{\Delta x}{2})}e^{i\beta_m z}e^{i\omega_m(t+\Delta t)} - e^{i\alpha_m(x-\frac{\Delta x}{2})}e^{i\beta_m z}e^{i\omega_m(t+\Delta t)}\}$$
$$+\frac{W_0^m}{\Delta z}\{e^{i\alpha_m x}e^{i\beta_m(z+\frac{\Delta z}{2})}e^{i\omega_m(t+\Delta t)} - e^{i\alpha_m x}e^{i\beta_m(z-\frac{\Delta z}{2})}e^{i\omega_m(t+\Delta t)}\} = 0 \tag{C1}$$

$$g\frac{\Theta_0^m}{2}\{e^{i\alpha_m x}e^{i\beta_m(z+\Delta z)}e^{i\omega_m(t+\Delta t)} + e^{i\alpha_m x}e^{i\beta_m z}e^{i\omega_m(t+\Delta t)}\}$$
$$+\frac{P_0^m}{\Delta z}\{e^{i\alpha_m x}e^{i\beta_m(z+\frac{\Delta z}{2})}e^{i\omega_m(t+\Delta t)} - e^{i\alpha_m x}e^{i\beta_m(z-\frac{\Delta z}{2})}e^{i\omega_m(t+\Delta t)}\} = 0 \tag{C2}$$

$$\frac{U_0^m}{\Delta t}\{e^{i\alpha_m(x+\frac{\Delta x}{2})}e^{i\beta_m z}e^{i\omega_m(t+\Delta t)} - e^{i\alpha_m(x+\frac{\Delta x}{2})}e^{i\beta_m z}e^{i\omega_m t}\}$$
$$+\frac{P_0^m}{\rho_0\Delta x}\{e^{i\alpha_m(x+\Delta x)}e^{i\beta_m z}e^{i\omega_m t} - e^{i\alpha_m x}e^{i\beta_m z}e^{i\omega_m t}\} = 0 \tag{C3}$$

$$\frac{\Theta_0^m}{\Delta t}\{e^{i\alpha_m x}e^{i\beta_m z}e^{i\omega_m(t+\Delta t)} - e^{i\alpha_m x}e^{i\beta_m z}e^{i\omega_m t}\}$$
$$+\frac{W_0^m}{2}\frac{\partial\overline{\rho}}{\partial z}[\theta\{e^{i\alpha_m x}e^{i\beta_m(z+\frac{\Delta z}{2})}e^{i\omega_m(t+\Delta t)} - e^{i\alpha_m x}e^{i\beta_m(z-\frac{\Delta z}{2})}e^{i\omega_m(t+\Delta t)}\}$$
$$+(1-\theta)\{e^{i\alpha_m x}e^{i\beta_m(z+\frac{\Delta z}{2})}e^{i\omega_m t} - e^{i\alpha_m x}e^{i\beta_m(z-\frac{\Delta z}{2})}e^{i\omega_m t}\}] = 0 \tag{C4}$$

Divide Equations (C1)–(C4) by $e^{i\alpha_m x}e^{i\beta_m z}$, then note $\lambda = e^{i\omega_m\Delta t}$, i.e. Equation (39), and rearrange:

$$\frac{U_0^m}{\Delta x}(e^{i\alpha_m\Delta x/2} - e^{-i\alpha_m\Delta x/2}) + \frac{W_0^m}{\Delta z}(e^{i\beta_m\Delta z/2} - e^{-i\beta_m\Delta z/2}) = 0 \tag{C5}$$

$$g\frac{\Theta_0^m}{2}(e^{i\beta_m\Delta z/2} + e^{-i\beta_m\Delta z/2}) + \frac{P_0^m}{\Delta z}(e^{i\beta_m\Delta z/2} - e^{-i\beta_m\Delta z/2}) = 0 \tag{C6}$$

$$\frac{U_0^m}{\Delta t}(\lambda - 1) + \frac{P_0^m}{\rho_0\Delta x}(e^{i\alpha_m\Delta x/2} - e^{-i\alpha_m\Delta x/2}) = 0 \tag{C7}$$

$$\frac{\Theta_0^m}{\Delta t}(\lambda - 1) + \frac{W_0^m}{2}\frac{\partial\overline{\rho}}{\partial z}[\{\theta(\lambda - 1) + 1\}\{e^{i\beta_m\Delta z/2} + e^{-i\beta_m\Delta z/2}\}] = 0 \tag{C8}$$

Recalling the identities

$$e^{i\beta\Delta z/2} + e^{-i\beta\Delta z/2} = 2\cos\left(\frac{\beta\Delta z}{2}\right) \tag{C9}$$

$$e^{i\beta\Delta z/2} - e^{-i\beta\Delta z/2} = 2i\sin\left(\frac{\beta\Delta z}{2}\right) \tag{C10}$$

DOI: 10.1002/fld

Equations (C5)–(C8) can be written as

$$\frac{U_0^m}{\Delta x}\sin\left(\alpha_m\frac{\Delta x}{2}\Big/2\right)\frac{W_0^m}{\Delta z}\sin\left(\beta_m\frac{\Delta z}{2}\right)=0 \tag{C11}$$

$$g\Theta_0^m\cos\left(\beta_m\frac{\Delta z}{2}\right)+\frac{2\mathrm{i}P_0^m}{\Delta z}\sin\left(\beta_m\frac{\Delta z}{2}\right)=0 \tag{C12}$$

$$\frac{U_0^m}{\Delta t}(\lambda-1)+\frac{2\mathrm{i}P_0^m}{\rho_0\Delta x}\sin\left(\alpha_m\frac{\Delta x}{2}\Big/2\right)=0 \tag{C13}$$

$$\frac{\Theta_0^m}{\Delta t}(\lambda-1)+W_0^m\frac{\partial\overline{\rho}}{\partial z}\left[\{\theta(\lambda-1)+1\}\cos\left(\beta_m\frac{\Delta z}{2}\right)\right]=0 \tag{C14}$$

Equations (C11)–(C14) can be written in a matrix form $\overline{\overline{A}}\cdot\overline{v}=0$ where

$$\overline{\overline{A}}=\begin{bmatrix} \dfrac{\sin\left(\alpha_m\frac{\Delta x}{2}\right)}{\Delta x} & \dfrac{\sin\left(\beta_m\frac{\Delta z}{2}\right)}{\Delta z} & 0 & 0 \\ 0 & 0 & \dfrac{2\mathrm{i}}{\Delta z}\sin\left(\beta_m\frac{\Delta z}{2}\right) & g\cos\left(\beta_m\frac{\Delta z}{2}\right) \\ \dfrac{(\lambda-1)}{\Delta t} & 0 & \dfrac{2i}{\rho_0\Delta x}\sin\left(\alpha_m\frac{\Delta x}{2}\right) & 0 \\ 0 & \dfrac{\partial\overline{\rho}}{\partial z}\left[\{\theta(\lambda-1)+1\}\cos\left(\beta_m\frac{\Delta z}{2}\right)\right] & 0 & \dfrac{(\lambda-1)}{\Delta t} \end{bmatrix} \tag{C15}$$

and

$$\overline{v}^{\mathrm{T}}=[U_0^m, W_0^m, P_0^m, P_0^m] \tag{C16}$$

For solutions other than the trivial $\overline{v}=0$ it is necessary that $|\overline{\overline{A}}|=0$, which provides the characteristic equation

$$\lambda^2+(\theta B^2-2)\lambda+(1+B^2[1-\theta])=0 \tag{C17}$$

where

$$B=N\Delta z\frac{\Delta t}{\Delta x}\sin\left(\alpha_m\frac{\Delta x}{2}\right)\cot\left(\beta_m\frac{\Delta z}{2}\right) \tag{C18}$$

i.e. the characteristic equation, (40), for the baroclinic forward-time method.

ACKNOWLEDGEMENTS

This work was partially funded by the University of Granada (‘*Plan Propio de Investigación UGR*’). Part of the numerical simulations was conducted in the computer facilities at SAIT (U.P. Cartagena).

DOI: 10.1002/fld

REFERENCES

1. Casulli V, Cheng RT. Semi-implicit finite difference methods for three-dimensional shallow water flow. *International Journal for Numerical Methods in Fluids* 1992; **15**:629–648.
2. Appt J, Imberger J, Kobus H. Basin-scale motion in stratified upper lake constance. *Limnology and Oceanography* 2004; **49**(4):919–933.
3. Shchepetkin AF, McWilliams JC. The regional ocean modeling system (ROMS): a split–explicit, free-surface, topography-following coordinates ocean model. *Ocean Modelling* 2005; **9**:347–404.
4. Yuan H, Wu CH. A two-dimensional vertical non-hydrostatic σ model with an implicit method for free-surface flows. *International Journal for Numerical Methods in Fluids* 2004; **44**:811–835.
5. Blumberg AF, Mellor GL. A description of a three-dimensional coastal ocean circulation model. In *Three-dimensional Coastal Ocean Models*, Heaps S (ed.). American Geophysical Union: Washington, DC, 1987; 1–16.
6. Griffies S, Böning C, Bryan F, Chassignet E, Gerdes R, Hasumi H, Hirst A, Treguier A-M, Webb D. Developments in ocean climate modeling. *Ocean Modelling* 2000; **2**:123–192.
7. Campin JM, Adcroft A, Hill C, Marshall J. Conservation properties in a free-surface model. *Ocean Modelling* 2004; **6**:221–244.
8. Rueda FJ, Cowen EA. Residence time of a freshwater embayment connected to a large lake. *Limnology and Oceanography* 2005; **50**(5):1638–1653.
9. Zaker NH, Imberger J, Pattiaratchi C. Numerical simulation of the coastal boundary layer off Perth, Western Australia. *Journal of Coastal Research* 2002; **18**(3):470–485.
10. Casulli V, Cattani E. Stability, accuracy and efficiency of a semi-implicit method for three-dimensional shallow water flow. *Computers and Mathematics with Applications* 1994; **27**(4):99–112.
11. Casulli V, Stelling G. Numerical simulation of 3D quasi-hydrostatic, free-surface flows. *Journal of Hydraulic Engineering* 1998; **124**(7):678–686.
12. Casulli V. A semi-implicit finite difference method for non-hydrostatic, free-surface flows. *International Journal for Numerical Methods in Fluids* 1999; **30**(4):425–440.
13. Casulli V, Walters RA. An unstructured grid, three-dimensional model based on the shallow water equations. *International Journal for Numerical Methods in Fluids* 2000; **32**(3):331–348.
14. Ahsan AKMQ, Blumberg AF. Three-dimensional hydrothermal model of Onondaga lake, New York. *Journal of Hydraulic Engineering* (ASCE) 1999; **125**(9):912–923.
15. Hodges BR, Imberger J, Saggio A, Winters K. Modeling basin-scale internal waves in a stratified lake. *Limnology and Oceanography* 2000; **45**(7):1603–1620.
16. Rueda FJ, Schladow SG, Palmarsson SO. Basin-scale internal wave dynamics during a winter cooling period in a large lake. *Journal of Geophysical Research—Oceans* 2003; **108**(C3):Art No. 3097.
17. Chen XJ. A free surface correction method for simulating shallow water flows. *Journal of Computational Physics* 2003; **189**:557–578.
18. Hodges BR. Accuracy order of Crank–Nicolson discretization for hydrostatic free surface flow. *Journal of Engineering Mechanics* 2004; **130**(8):904–910.
19. Gross ES, Casulli V, Bonaventura L, Koseff JR. A semi-implicit method for vertical transport in multidimensional models. *International Journal for Numerical Methods in Fluids* 1998; **28**:157–186.
20. Robson BJ, Hamilton DP. Three-dimensional modelling of a microcystis bloom event in the Swan river estuary, Western Australia. *Ecological Modelling* 2004; **174**(1–2):203–222.
21. Laval B, Imberger J, Hodges BR, Stocker R. Modeling circulation in lakes: spatial and temporal variations. *Limnology and Oceanography* 2003; **48**(3):983–994.
22. Gross ES, Koseff JR, Monismith SG. Three-dimensional salinity simulations of south San Francisco Bay. *Journal of Hydraulic Engineering* (ASCE) 1999; **125**(11):1199–1209.
23. Eliason DE, Bourgeois AJ. Validation of numerical shallow water models for stratified seiches. *International Journal for Numerical Methods in Fluids* 1997; **24**:771–786.
24. Kowalik Z, Murty TS. *Numerical Modeling of Ocean Dynamics*. World Scientific: Singapore, 1993; 480.
25. Gross ES, Bonaventura L, Rosatti G. Consistency with continuity in conservative advection schemes for free-surface models. *International Journal for Numerical Methods in Fluids* 2002; **38**:307–372.
26. Gray WG, Lynch DR. Time-stepping schemes for finite element tidal model computations. *Advances in Water Resources* 1977; **1**:83–95.
27. Leendertse JJ. Aspects of a computational model for long period water-wave propagation. *Rand Memorandum RM-5294-PR*, Santa Monica, 1967.

DOI: 10.1002/fld

28. Cushman-Roisin B. *Introduction to Geophysical Fluid Dynamics*. Prentice-Hall: Englewood Cliffs, NJ, 1994; 320.
29. Hodges BR, Laval B, Wadzuk BM. Numerical error assessment and a temporal horizon for internal waves in a hydrostatic model. *Ocean Modelling* 2006; **13**(1):44–64. doi:10.1016/j.ocemod.2005.09.005
30. Laval B, Hodges BR, Imberger J. Numerical diffusion in 3D, hydrostatic, Z-level, lake models. *Journal of Hydraulic Engineering* (ASCE) 2003; **129**(3):215–224.
31. Leonard BP. A stable and accurate convective modelling procedure based on quadratic upstream interpolation. *Computer Methods in Applied Mechanics and Engineering* 1979; **19**(1):59–98.
32. Hodges BR, Rueda FJ. Linear accuracy and stability of semi-implicit two-level predictor-corrector methods for hydrostatic barotropic/baroclinic flows. *International Journal for Numerical Methods in Fluids* 2006, submitted for publication.
33. Camassa R, Holm D. Dispersive barotropic equations for stratified mesoscale ocean dynamics. *Physica D* 1992; **60**:1–15.

DOI: 10.1002/fld